MULTISCALE IMAGE TEXTURE ANALYSIS IN WAVELET SPACES

M. H. Groß, R. Koch, L. Lippert, A. Dreger

Computer Science Department
ETH–Zürich, CH–8092 Zürich
Switzerland
E–mail: grossm@inf.ethz.ch

ABSTRACT

This paper describes a new method for texture feature extraction and analysis in images using Wavelet transform (WT), KL–Expansion and Kohonen maps. For this purpose, we first apply a global wavelet transform on the initial image. Due to the localization properties of the WT both in the spatial and in the frequency domain it is possible to describe the local texture features in the surroundings of any pixel by a set of respective wavelet coefficients. This is accomplished by a local traversal of the wavelet pyramid and finally results in the feature vector we look for. Since the localization is limited by Heisenberg's uncertainty principle we have to approximate the single coefficients for each pixel by picewise linear interpolation. Once the feature vector is derived from the WT, further steps in our analysis pipeline perform decorrelation, normalization and finally clustering and supervised classification.

In contrast to many related wavelet–based approaches, that usually apply different WT's on every texture sample and classify based on means derived from the former, our method especially accounts for many real world applications. In those cases we usually do not face large coherent texture regions that allow separated treatment. Moreover our approach employs a global WT and then stresses the local properties of the basis functions to identify local areas of interest from the initial image, as for instance training areas. We illustrate the efficiency of the method by classifying different real world textures with LVQ classifiers.

1. INTRODUCTION

Texture analysis is a very important method for the interpretation and classification of grey level images and a lot of effort has been spent so far, to derive appropriate and meaningful texture features for classification purposes. The early approaches were mainly influenced by statistical measures derived from the intensity distribution in the texture. [2] for instance, investigated different statistical texture features for classification purposes and [3] reported on the correspondence between second order statistics in textures and the discrimination performance of the human visual system. Following the mathematical formulation of the wavelet–transform ([8], [9], [10]) recent work has been focussed on the investigation of multiresolution analysis techniques for texture feature extraction. [4] used Gabor–functions of different spectral ranges and orientations to derive a multiscale sight onto the texture. [5] employed a set of local linear transforms as an initial step in a texture recognition pipeline and combined them with dimensionality reduction techniques. Orthogonal wavelets and wavelet packages for texture analysis had been introduced by [6] and [7]. In particular, the tree–structured approach seems to be favorable since it operates very successfully on a set of Brodatz–textures.

However, most approaches derive global wavelet features in terms of means from a specific type of texture and they transform each subset separately into the wavelet space. This procedure renders high classification rates but it neither takes into account texture boundaries nor does it take advantage of the spatial localization of the wavelet transform. Consequently, for many practical applications, as for instance remote sensing or medical imaging, difficulties will arise in applying these techniques because they don't provide large spatial coherent textures.

The following paper reports on a different approach to derive texture features from wavelet–transform using the spatial and frequency localization of the WT. The idea is to apply first a global transform on the initial image consisting of different types of textures. Due to the local properties of the WT it is possible to describe local texture features within respective training areas by means of a set of wavelet coefficients. This feature vector can be used for further texture analysis steps. In particular we employ a principal component analysis for dimensionality reduction and a Kohonen–based learning vector quantization (LVQ) classifier [1] to discriminate the different classes of textures. We investigate the classification and generalization behavior of this approach for different images each consisting of four different texture types, as Brodatz, random dots and sine gratings. A comparison is given between the performance of Haar–, Battle–Lemarie–, Daubechies–wavelets and Gabor–functions and the impact of the PCA is described. Finally, we illustrate the method by applications on SAR– and MR images.

2. THE WAVELET TRANSFORM

2.1. Mathematical Foundations

The WT is a linear integral transform that maps $L^2(\mathbb{R}) \rightarrow L^2(\mathbb{R}^2)$. But in contrast to the Fourier transform, it is both located in time/space and in frequency [11],[16]. The continuous WT (CWT) is defined as the inner product

$$W_f(a,b) := \int_{-\infty}^{\infty} \psi_{ab}(t)\, \bar{f}(t) dt = \langle \psi_{ab}, f \rangle \qquad (1)$$

where

$$\psi_{ab}(t) := \frac{1}{\sqrt{|a|}} \psi\left(\frac{t-b}{a}\right) \qquad a,b \in \mathbb{R},\ a \neq 0 \qquad (2)$$

and orthonormal wavelets have to satisfy [8]

$$\int_0^{\infty} \frac{|\hat{\psi}(\omega)|^2}{\omega} d\omega < \infty \qquad (\hat{\psi}(\omega) \ \textit{is the FT of} \ \psi(t)) \qquad (3)$$

Equation (3) implies the required condition for orthonormal basis functions namely

$$\hat{\psi}(0) = \int_{-\infty}^{\infty} \psi(t) dt = 0 \quad \text{(band–bass characteristics)} \qquad (4)$$

A discrete orthonormal wavelet representation is then defined by

$$\psi_{mn}(t) := a_0^{-\frac{m}{2}} \psi\left(a_0^{-m} t - n b_0\right) \qquad (5)$$

with $a = a_0^m, b = n\, b_0\, a_0^m$. For the discrete WT we obtain

$$W_f^d(m,n) := \int_{-\infty}^{\infty} \psi_{mn}(t)\bar{f}(t)dt = \langle \psi_{mn}, f \rangle \quad m,n \in \mathbf{Z} \quad (6)$$

The selection of $a_0 = 2$ and $b_0 = 1$ scales the transform onto a dyadic grid. Orthonormality of the basis functions is defined through the inner product

$$\langle \psi_{mn}, \psi_{\tilde{m}\tilde{n}} \rangle = \int_{-\infty}^{\infty} \psi_{mn}(t)\psi_{\tilde{m}\tilde{n}}(t)dt = \delta_{m\tilde{m}}\delta_{n\tilde{n}} \quad (7)$$

$$\text{with} \quad \delta_{ij} := \begin{cases} 1 & \text{if } i = j \\ 0 & \text{else} \end{cases}$$

In order to build orthonormal wavelet bases [13] and [10] propose the definition of the following function spaces. Their orthonormal bases are derived by scaling and shifting respective prototypes ϕ and ψ.

$$V_m := \overline{span\{\phi_{mn} | n \in \mathbf{Z}\}}$$
$$\text{and} \quad O_m := \overline{span\{\psi_{mn} | n \in \mathbf{Z}\}}, V_m, O_m \subset L^2(\mathbb{R}) \quad (8)$$
$$\phi_{mn} := 2^{-\frac{m}{2}}\phi(2^{-m}t - n) \text{ and } \psi_{mn} := 2^{-\frac{m}{2}}\psi(2^{-m}t - n)$$

ϕ is the so–called scaling function and ψ the wavelet.
This set of multiresolution function spaces $(V_m)_{m\in\mathbf{Z}}$ can be derived from each other by using the orthonormal complements O_m in each resolution step in

$$V_{m-1} = V_m \oplus O_m \quad (9)$$

In order to decompose any discrete signal $\left(c_j^0\right)_{j\in\mathbf{Z}}$ it is first projected into V_0

$$f(t) := \sum_j c_j^0 \phi_{0j}(t) \quad f(t) \in V_0 \quad (10)$$

The computation of the decomposed signals $\left(c_j^1\right)_{j\in\mathbf{Z}}$ and $\left(d_j^1\right)_{j\in\mathbf{Z}}$

$$f(t) = \sum_j c_j^1 \phi_{1j}(t) + \sum_j d_j^1 \psi_{1j}(t) \quad (11)$$

decreases the resolution by a factor of 2. The corresponding coefficients are then obtained following equation (6). Due to the spectral properties of ϕ and ψ, $\left(c_j^1\right)_{j\in\mathbf{Z}}$ can be interpreted as the low–pass part of $\left(c_j^0\right)_{j\in\mathbf{Z}}$ where $\left(d_j^1\right)_{j\in\mathbf{Z}}$ represents the difference signal. Equation (9) proposes an iterated scheme to decompose the function into a low–pass part and a difference signal. This iterated decomposition scheme can be illustrated by the pyramid of figure 1a.

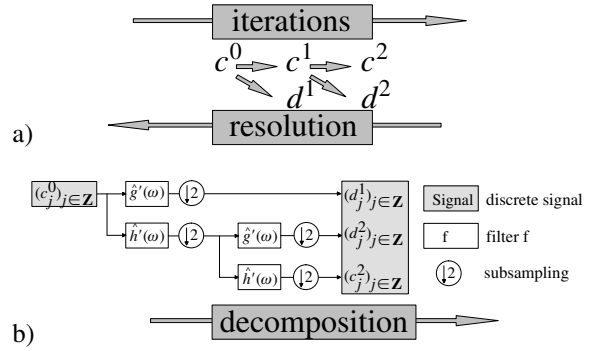

Fig. 1: a) Resolution pyramid for the iterated decomposition of the signal $\left(c_j^0\right)_{j\in\mathbf{Z}}$
b) QMF–subband coding scheme for the WT

The implementation of the WT can be accomplished by computation of the inner products in equation (6) or implicitly by so–called quadrature mirror pair filters (QMFs), depending on whether the wavelets are given explicitly. This scheme is illustrated in figure 1b. It can be proofed [10] that the low–pass signal $\left(c_j^m\right)_{j\in\mathbf{Z}}$ and the difference signals $\left(d_j^m\right)_{j\in\mathbf{Z}}$ are derived from an iterated filtering of the initial signal $\left(c_j^0\right)_{j\in\mathbf{Z}}$ using the filter pairs $\hat{h}'(\omega) = \sum_{n=-\infty}^{\infty} h(-n)e^{in\omega}$ and $\hat{g}'(\omega) = e^{-i\omega}\overline{\hat{h}'(\omega + \pi)}$ with $h(n) := 2^{-\frac{1}{2}} \int_{-\infty}^{\infty} \phi\left(\frac{x}{2}\right)\phi(x - n)dx.$

Separable extensions of the WT to multiple dimensions are constructed straightforwardly from the n–dimensional function spaces $V_m^n, O_m^n \subset L^2(\mathbb{R}^n)$, given by the tensor products

$$V_{m-1}^n := \bigotimes_{i=1}^{n} V_{m-1} = \bigotimes_{i=1}^{n} (V_m \oplus O_m) \quad (12)$$

The two–dimensional extensions of equations (10) and (11) yield:

$$f(x,y) := \sum_{j,k} c_{jk}^0 \phi_{0jk}(x,y) \quad f(x,y) \in V_0^2 \quad (13)$$

$$f(x,y) = \sum_{j,k} c_{jk}^1 \phi_{1jk}(x,y) + \sum_{l=1}^{3} \sum_{j,k} d_{jk}^{1,l} \psi_{1jk}^l(x,y) \quad (14)$$

The tensor products from equation (12) cause an orientation selectivity of the difference signals $(d_{jk}^{1,1})$,$(d_{jk}^{1,2})$ and $(d_{jk}^{1,3})$ emphasizing the horizontal, vertical and diagonal components respectively.

2.2. Wavelet Bases for Texture Analysis

The different wavelet bases we employ for our method can be divided into orthonormal ones and non–orthogonal ones. Whereas orthonormal wavelets allow a compact coding and a perfect reconstruction of the image on the one side, a trade–off has to be found between smoothness of the function, its shape and a strict finite support of the wavelet on the other side. Furthermore, many researches [5] use Gabor functions as oriented filters for texture analysis since they are perfectly smooth and allow a dense staggering of the orientations. For this reason the following different types of wavelets are compared in the investigation reported in this paper.

2.2.1. Haar Wavelets

A very simple, but discontinuous basis is given with the Haar wavelet, whose scaling function is defined by

$$\phi(t) := \begin{cases} 1 & \text{for } 0 \le t < 1 \\ 0 & \text{else} \end{cases} \quad (15)$$

The Fourier transform of this function equation (16) shows, that this wavelet has optimal localization properties in the spatial domain on the one hand

$$\hat{\phi}(2\omega) = e^{-i\omega}\frac{\sin(\omega)}{\omega} \quad (16)$$

but on the other hand a rather bad localization in frequency.

2.2.2. Daubechies Wavelets

In order to obtain better localization in frequency along with a minimal local support in space and smoother basis functions, Daubechies [13] proposes wavelet types as follows: The regularity of the scaling function is defined as the maximum value of r such that

$$|\hat{\phi}(\omega)| \le \frac{c}{(1 + |\omega|)^{r+1}} \qquad c \in \mathbb{R}^+ \quad (17)$$

This relation also describes the continuity of $\phi(t)$, where $\phi(t) \in C^i(\mathbb{R})$ with $i \le r$. The regularity of the Daubechies wave-

lets is proportional to the number of vanishing moments N, defined by

$$\int_{-\infty}^{\infty} t^n \psi(t)dt = 0 \quad n \in \{0,\ldots,N\} \tag{18}$$

The function is only constrained by equation (19).

$$\int_{-\infty}^{\infty} \phi(t)dt = 1 \tag{19}$$

2.2.3. Coiflet – Bases

Restricting further the scaling function to a fixed number of vanishing moments the following equation (20)

$$\int_{-\infty}^{\infty} t^n \phi(t)dt = 0 \quad n \in \{1,\ldots,N'\} \tag{20}$$

results in a different wavelet type, the so–called Coiflet wavelet [11]. Except the Haar–wavelet one of the basic properties of bases with a strict local support is a lack of symmetry. However, there is a relationship between the number of vanishing moments, stated earlier, and the symmetry of the function. Thus Coiflet bases appear to be "more symmetric" than the Daubechies ones.

2.2.4. Battle–Lemarie Wavelets

Wavelets with infinite support can be approximated in the frequency plane. An example is given by equ. (21) – (24) (see [10]).

$$\hat{\phi}(\omega) := \frac{1}{\omega^n \sqrt{\Sigma_8(\omega)}} \tag{21}$$

where

$$\Sigma_8(\omega) := \frac{N_1(\omega) + N_2(\omega)}{105\left(\sin\frac{\omega}{2}\right)^8} \tag{22}$$

with

$$N_1(\omega) := 5 + 30\left(\cos\frac{\omega}{2}\right)^2 + 30\left(\sin\frac{\omega}{2}\right)^2\left(\cos\frac{\omega}{2}\right)^2 \tag{23}$$

and (24):

$$N_2(\omega) := 2\left(\sin\frac{\omega}{2}\right)^4\left(\cos\frac{\omega}{2}\right)^2 + 70\left(\cos\frac{\omega}{2}\right)^4 + \frac{2}{3}\left(\sin\frac{\omega}{2}\right)^6$$

This wavelet type is often referred in literature as the Battle–Lemarie wavelet.

2.2.5. Gabor Wavelets

As we stated earlier, Gabor functions have approved to be very successful for many approaches in multidimensional signal analysis, since they can serve as locally oriented filters and allow a dense angular staggering along with optimal smoothness in space and frequency. They are often described as

$$\psi_{\vec{k}}(\vec{t}) = \frac{1}{\sqrt{\pi}\frac{u}{|\vec{k}|}} e^{i\vec{k}^T\vec{t}} e^{\frac{-|\vec{k}|^2\vec{t}^T\vec{t}}{2u^2}} \tag{25}$$

with

$$\vec{k}(j,l) = \frac{2\pi}{N}\sqrt{2^j}\begin{bmatrix}\cos\left(\pi\frac{l}{L}\right)\\ \sin\left(\pi\frac{l}{L}\right)\end{bmatrix} \tag{26}$$

where $\frac{u}{|\vec{k}|}$ represents the variance of the Gaussian. For our investigations we fix L=16, $l \in \{0,...,7\}$ and $j \in \{0,...,2\log_2 N - 1\}$. This results in a "semi–dyadic" scaling for each frequency range and an angular discretization of $\frac{\pi}{4}$.

2.3. Examples

The following figure 2 again illustrates the shapes of a separable extension of a Daubechies 4–tap wavelet we built using the tensor products of equation (12). Upper left, the scaling function is presented. The other pictures represent the three mother wavelets that account for the different directional components of the signal. It is clearly to see where the name of this transform is derived from.

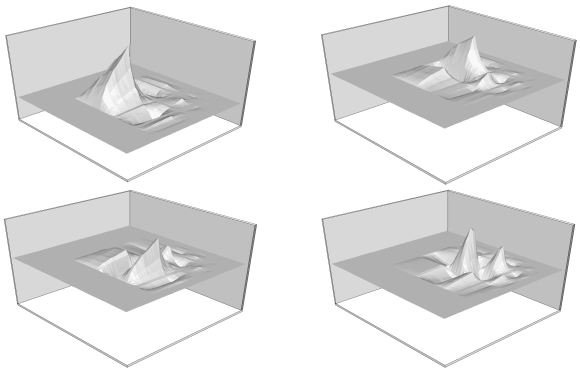

Fig. 2: Separable 2D–extensions built from a 4–tap Daubechies wavelet; scaling function upper left and spatially oriented wavelets.

3. IMPLEMENTATIONS

3.1. A Pipeline for Texture Analysis

The pipeline we employ for our investigations follows the illustrations of figure 3. First of all, a global wavelet–transform is applied on the initial grey level image. After defining training sets in the different texture samples of the image, it is possible to characterize the local texture properties using the respective coefficients of the WT. In order to rank the different dimensions of the feature vector according to their significance, we apply a principal component analysis (PCA) and limit the number of dimensions minimizing the information loss. Finally, a neural network that bases on Kohonen's LVQ classifies and generalizes the trained texture types.

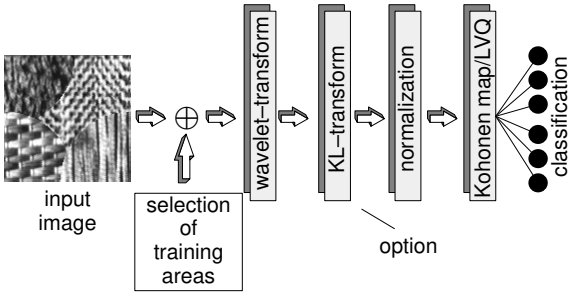

Fig. 3: Texture analysis pipeline used for the investigation

This scheme allows the definition of arbitrary training areas in large scale images, as for instance remotely sensed data, and it eases the access to the local texture features.

3.2. Deriving local Texture Features from Images

The result of the wavelet transform is a pyramidal representation of the image as illustrated in figure 4b. The initial image is separated into a dyadic set of frequency channels where horizontal, vertical and diagonal components are split by the corresponding wavelet. Due to the local properties of the wavelet transform, it is

possible to derive local texture features in the adjacency of any pixel (x_i, y_i) of the initial image by a set of respective coefficients from the pyramid. Supposing a depth of N in the pyramid, the set $g(x_i, y_i)$ renders a feature vector for further analysis:

$$\mathbf{g}(x_i, y_i) = \begin{cases} \left\{ d^{m,l}_{x_i y_i} \mid l = 1 + (i \bmod 4) \right\} & \text{if } (i \bmod 4 \le 2) \\ \left\{ c^{m}_{x_i y_i} \right\} & \text{else} \end{cases}$$

$$m := 1 + \left\lfloor \frac{i}{4} \right\rfloor$$

Since the spatial localization of the WT decreases with lower frequencies according to the Heisenberg principle, we have to perform a bilinear interpolation between adjacent coefficients in every channel to approximate the contribution of the respective wavelet for a spatial coordinate (x_i, y_i) in the image.

Figure 4 again illustrates these properties of the WT. The initial image consisting of different types of textures is transformed into the wavelet space. The result is a 4 level pyramid that separates horizontal, vertical and diagonal subbands of different spectral ranges. The local texture properties of the image can be described by the respective wavelet coefficients of the pyramid. The contribution of the corresponding sets $\mathbf{g}(x_i, y_i)$ can be demonstrated by the reconstruction of the image using only the low–pass coefficients of the pyramid and the $\mathbf{g}(x_i, y_i)$ inside the marked region. The resulting image in figure 4c is varying its spatial resolution, since only inside the rectangle the higher frequency information is provided.

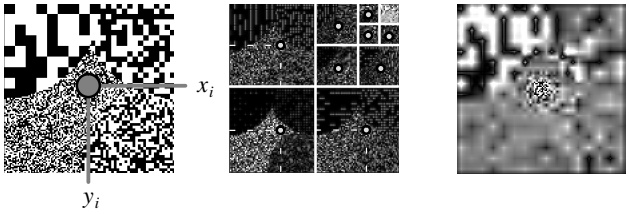

Fig. 4: a) Initial test image consisting of four different texture types and non–linear texture boundaries
b) Subband representation by an orthogonal WT (Battle–Lemarie filter [10])
c) Reconstruction of the image with a spatially varying resolution.

It should be noted, that we add the coefficients of the scaling function of each resolution step $c^{m}_{x_i y_i}$ into our feature vector. They represent the low–pass parts of the signal and are decomposed further. This gives rise to a correlation of the single features on the one side, but on the other side it turned out to provide better results. For this end, decorrelation is a meaningful step in our pipeline even when employing orthonormal wavelet types.

3.3. Dimensionality Reduction, Normalization and Classification

As stated earlier, decorrelation is required to provide an optimal representation of the extracted features. There are many different approaches in mathematical statistics to perform this. The method proposed here employs the PCA [14]. Since the class density distribution of the data is unknown, the normalization step supposes an uniform distribution and scales the data straightforwardly to its minimum and its maximum.

The required cluster analysis of the texture features as well as the supervised classification step is accomplished with an extension of the Kohonen Feature Map proposed by [1]. The basic topology of the network is illustrated in figure 5. The competitive layer is extended to 3D and each neuron c is assigned to a specific color triplet (R_c, G_c, B_c) in the RGB color space. During the non–supervised organization process the network performs a c–means clustering of the incoming data, where each weight vector $\mathbf{w}_j$ represents the position of a centroid in feature space. Since the network tries to preserve the data topology, neighbored neurons in the output layer are mapped to neighbored cluster centers in feature space. Visualizing these cluster centers for each image pixel to be analyzed, in terms of color, results in a mapping of a multidimensional data distribution to color similarities in RGB. The updating of the weights $\mathbf{w}_j$ for each neuron j during learning follows the basic rules of Kohonen [15]:

$$\Delta w_{ij} = \alpha(t) \cdot (g_i - w_{ij}) \;, \quad \text{if neuron } j \in N_j(t) \qquad (27)$$

$\alpha(t)$: time dependent learning rate
g_i: feature coordinate i

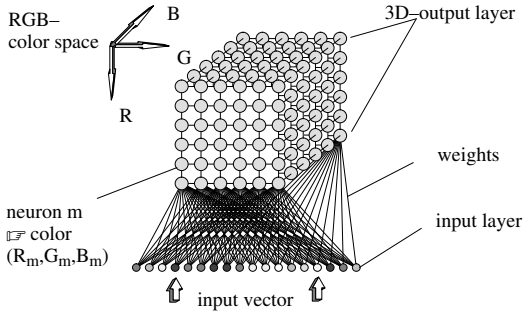

Fig. 5: 3D Kohonen map and color assignment

$N_m(t)$ represents the local neighborhood of neuron m with the minimum Euklidian distance to the feature vector $\boldsymbol{g}$.

Once the network is organized, the Learning Vector Quantization allows for supervised classification. This procedure first assigns a class to each neuron based on the majority voting on the training data. But however the weights of the network approximate the initial data density distribution rather than optimal (Bayesian) decision boundaries. As a result of this neurons close to the class boundaries are then shifted towards a minimum error boundary. We trained the network with 100000 cycles unsupervised and with 50000 LVQ cycles for our purpose, ($\alpha = 0.2$).

4. RESULTS

Figure 6 shows four different images we generated to investigate the capabilities of our approach. The task was to classify each image after training the pipeline with samples that are derived from specific training sets. The following wavelets were compared to each other with regard to the classification and generalization behavior:

– Gabor wavelets (8 spatial orientations)
– Daubechies wavelets (4–tap)
– Haar wavelets
– Battle–Lemarie wavelets

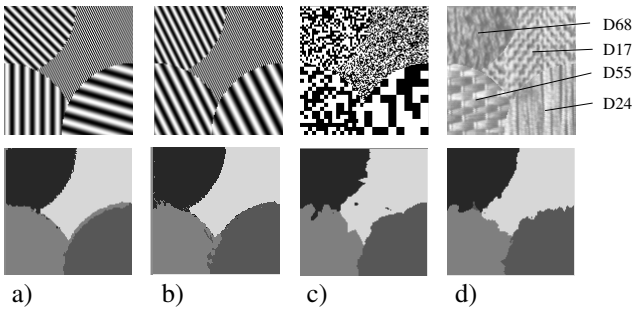

Fig. 6: Different texture compositions and results:
a) Sine1: Sine gratings of different spectral ranges and orientations
b) Sine2: Sine gratings of different spectral ranges
c) Random dots
d) Brodatz textures: D17, D24, D55, D68 [12]

The decomposition with orthonormal wavelets was performed up to 5 iterations resulting in a 20–dimensional feature vector. The Ga-

bor wavelets generated 45 coefficients at 5 iterations. The error recorded in the following diagrams was computed from the falsly assigned pixels within the training set and as well as from those regions not covered by training areas. Due to the dense arrangements of our training regions in the single textures, we can interpret the results as a reclassification performance.

Figure 7 illustrates the error we obtained for different images and wavelets as a function of the iteration depth. The results show that the accuracy depends on the texture type. The decorrelation of the features with the PCA was performed as a mapping to the 8 most significant eigenvectors for orthonormal wavelets and 18 for Gabor functions, respectively.

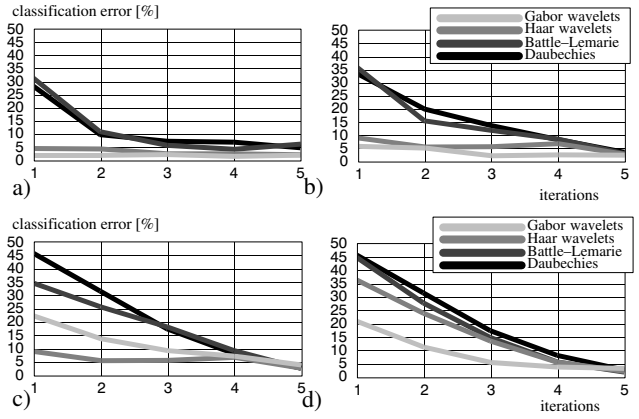

Fig. 7: results for a) SINE–1, b) SINE–2, c) RANDOT and d) BRODATZ

This is illustrated again in figure 8 that presents the best match for our examples and the influence of the PCA on the error as well. Figure 8a shows the best results. Due to the nonlinearity of the texture reagions the errors are mostly located close to their boundaries.

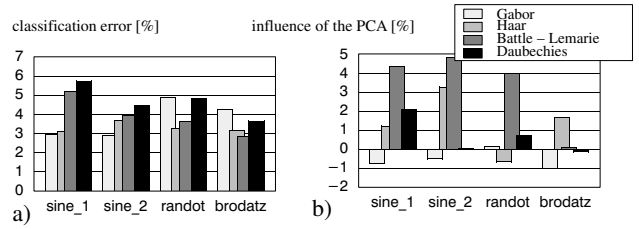

Fig. 8: a) best matches b) influence of the PCA

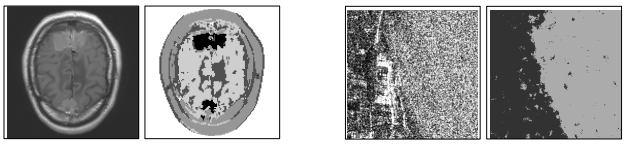

Fig. 9: Initial textures and best match
a) T_1–weighted MR image with two Menignoma
b) Classification result separating the tumors (7 classes are defined)
c) Seasat–SAR image of Northern Netherlands
d) Water–ground separation using Gabor wavelets

Finally, two applications are illustrated in figure 9. First a Seasat SAR image of the coast line of the Netherlands is shown as well as the result of a two–class water–ground separation. Furthermore, a T_1–weighted image slice of an MR scan is presented and the corresponding classification result. Further investigations include detailed studies on the generalization behavior of the method for the classification of brain tumors and SAR images.

5. CONCLUSIONS AND WORK IN PROGRESS

The method proposed in this paper promises a way for texture feature extraction in images using one unique and global transform. Generally it can be stated, that the errors in the investigated examples depend on both the wavelet type and on the image pyramid. The next two steps to do are to investigate the reliability of this method for larger images with more different textures included. Furthermore we have to record the generalization capabilities of our method. Since the error is related to the wavelet type, and to the texture type as well, we should combine different transforms from one image and decorrelate them to get better results. Finally the applications sketched above will be stressed in the future. In particular volumes require 3D analysis that could be embedded into a wavelet–based volume renderer.

6. ACKNOWLEDGEMENTS

Most of this research was done by the authors at the Computer Graphics Center in Darmstadt, Germany. It was supported in parts by the German Telekom within the KAMEDIN project.

7. LITERATURE

[1] Groß, M.; Seibert, F.: "Visualization of Multidimensional Image Data Sets using a Neural Network". The Visual Computer, Vol. 10, pp. 145 – 159, 1993

[2] Haralik, R.M.: "Statistical and Structural Approaches to Texture". Proceedings of the IEEE, Vol. 67, No. 5, pp.786 – 804, 1979

[3] Julesz, B.; Frisch, H. L.; Gilbert, E. L.; Shepp, L. A.: "Inability of Humans to Discriminate between Visual Textures that Agree in Second–Order Statistics – Revisited". Perception, Vol. 2, pp. 391 – 405, 1973

[4] Bovik, A. C.; Clark, M.; Geisler, W.: "Multichannel Texture Analysis Using Localized Spatial Filters". IEEE Transactions on Pattern Analysis and Machine Intelligence, Vol. 12, No. 1, pp. 55 – 73, 1990

[5] Unser, M.; Eden, M.: "Multiresolution Feature Extraction and Selection for Texture Segmentation". IEEE Transactions on Pattern Analysis and Machine Intelligence, Vol. 11, No. 7, pp. 717 – 728, 1989

[6] Laine,A.; Fan, J.: "Texture Classification by Wavelet Packet Signatures". IEEE Transactions on Pattern Analysis and Machine Intelligence, Vol. 15, No. 11, pp. 1186 – 1191, 1993

[7] Chang, T.; Kuo, C.: "Texture Analysis and Classification with Tree–Structured Wavelet Transform". IEEE Transactions on Image Processing, Vol. 2, No. 4, pp. 429 – 441, 1993

[8] Grossmann, A.; Morlet, J.: "Decomposition of Hardy Functions into Square Integrable Wavelets of Constant Shape". SIAM Journal of Mathematical Analysis, Vol. 15, pp. 723–736, 1984

[9] Daubechies, I.: "The Wavelet Transform, Time–Frequency Localization and Signal Analysis". IEEE Transactions on Information Theory, Vol. 36, pp. 961 – 1005, 1990

[10] Mallat, S.: "A Theory for Multiresolution Signal Decomposition: The Wavelet Representation". IEEE Transactions on Pattern Analysis and Machine Intelligence, Vol. 11, No. 7, pp. 674–693, July 1989

[11] A. N. Akansu, Richard A. Haddad "Multiresolution Signal Decomposition", AcademicPress, Inc., 1992

[12] P. Brodatz, Textures–A photographic album for artists and designerts. New York: Dover. 1966.

[13] I. Daubechies, "Orthonormal Bases of Compactly Supported Wavelets", Communications on Pure and Applied Mathematics, VOL XLI, pp 909–996, 1988

[14] K. Fukunaga, "Introduction to Statistical Pattern Recognition", 2nd Ed. Academic Press, 1990

[15] T. Kohonen, "The Self–Organizing Map", Proceedings of the IEEE, vol. 78, pp. 1464

[16] M. Vetterli "Wavelets and Filter Banks: Theory and Design", IEEE Trans. on Signal Proc., vol. 40, pp 2207–2231, 1992